Supplementary Materials for

Coherent Phonon Heat Conduction in Superlattices

Maria N. Luckyanova, Jivtesh Garg, Keivan Esfarjani, Adam Jandl, Mayank T. Bulsara, Aaron J. Schmidt, Austin J. Minnich, Shuo Chen, Mildred S. Dresselhaus, Zhifeng Ren, Eugene A. Fitzgerald, Gang Chen*

*To whom correspondence should be addressed. E-mail: gchen2@mit.edu

Published 16 November 2012, *Science* **338**, 936 (2012)
DOI: 10.1126/science.1225549

This PDF file includes:

Materials and Methods

Time-Domain Thermoreflectance Experiment

The superlattice (SL) samples were prepared using metal organic chemical vapor deposition (MOCVD) on undoped GaAs wafers oriented in the (001) direction. Prior to the SL growth, a 500 nm GaAs buffer layer was grown on the substrate. An aluminum layer was deposited using electron beam evaporation on the SL samples, on a sapphire sample, and on a piece of the GaAs substrate using electron beam evaporation. The thickness of the Al layer was measured using profilometry and verified with time-domain thermoreflectance (TDTR) measurements of the sapphire calibration sample. Both techniques yielded Al layer thicknesses within a 5 nm window of 100 nm.

Details of the TDTR experiment performed herein are given elsewhere (*43, 44*). Briefly, a high-powered pump pulse modulated to between 3 and 12 MHz for lock-in detection, impinged on the surface of the Al transducer and generated hot electrons at the surface. These hot electrons thermalized within tens of fs and sent a heat pulse propagating perpendicular to the SL interfaces. The heat diffused from the Al layer, through the SL, and into the substrate. A much weaker time-delayed probe pulse measured the changing reflectance of the Al layer caused by the changing surface temperature. By varying the delay time between 0 and 6 ns, we obtained a cooling curve that could be matched to a multidimensional, multilayer Fourier law analysis of the thermal transport, giving numerical results for the unknown thermal transport properties.

The samples were mounted into a cryostat under high ($\sim 10^{-5}$ torr) vacuum and were cooled using liquid He for low-temperature measurements. The temperature of the sample was measured using a Si diode in contact with the surface of the sample via thermal grease.

The thermal conductivity data presented in the main body of the manuscript represent the averages of approximately 60 individual thermoreflectance curves. Three thermoreflectance measurements were performed at five locations on each sample and at four different modulation frequencies: 3 MHz, 6 MHz, 9 MHz, and 12 MHz. No modulation frequency dependence was observed in the data, so all the data from the different frequencies were included in the averaging. In general, the standard deviation from the average is approximately 10%. Figures S1 A shows the same data as is given in the main body of the paper with standard deviation bars included. Figure S1 B shows a typical data set along with the fitting curve.

The cooling curve yielded by the experiment was fitted to the solution of the Fourier heat conduction equations applied to a multi-dimensional, multi-layer stack to determine the unknown parameters. In this case, the unknown parameters were the thermal interface conductance (TIC) between the Al optical transducer layer and the SL and the thermal conductivity, k, of the SL. The average of the heat capacities of AlAs and GaAs were used for the heat capacity of the SL. Separate measurements of the thermal properties of Al on a GaAs substrate provided an initial guess for the TIC. The interface conductance, which is highly dependent upon the sample quality, the deposition quality, and the

sample surface chemistry, was allowed to float to yield best fitting results. In order to determine whether the interface conductance was greatly affecting the results of the experiment, a sensitivity analysis was performed (*45*).

We should acknowledge that strictly speaking, however, fitting the experimental data using Fourier theory is not valid. Instead, the Boltzmann equation should be solved using scattering rates and phonon transmissions as input parameters. Such computations, however, are beyond current computational abilities. Past studies of one-dimensional pump-and-probe setups show that the Boltzmann equation can be fitted reasonably well by Fourier's law using a reduced thermal conductivity (*46*). In the worst case scenario for our experiment (300K for the 9 period SLs), we estimate that about 40% of the total thermal conductivity is contributed by ballistic phonons with frequencies below 1 THz, and they traverse the SL in 0.2 ns, which is much shorter than the 6 ns experimental time. The other 60% is contributed by diffusive phonons that can be reasonably described with the diffusive Fourier law. This explains why the Fourier law calculation can fit the experimental data reasonably well, as shown in Fig. S2. The effective thermal conductivity values extracted from the experimental study are used together with first-principle's and Green's functions simulations to reveal the coherent phonon transport mechanism.

For the thinnest sample at the lowest temperatures, where the interface conductance was expected to play the largest role, a representative sensitivity analysis is shown in Fig. S2 A. This analysis shows the sensitivity of the fitting of a 1-pd SL to both the thermal conductivity of the sample and the TIC at 30K and a modulation frequency of 6 MHz. The plot shows that the fitting is more sensitive to the thermal conductivity of the sample for all times. This result is understandable when one considers the dependence on heat capacity of the solution to the heat equation. The interface has no heat capacity while the layer itself has a finite heat capacity.

To further verify these results, we plot the data along with best fit lines (in blue) as well as lines of variation (in red and green for +/- variations) in Figs S2 B and C. These lines of variation show how much the fitting curve would change with a prescribed change in the value of a specific fitting parameter. Figure S2 B shows that with a 100% change in the interface conductance, the fitting curve does not change. However, Fig. S2 C shows that with just a 10% change in the thermal conductivity of the sample, the fitting curve does change. This analysis further verified that the fitting was more sensitive to the thermal conductivity of the SL rather than the TIC, thus providing confidence in the results of the experiment presented in the paper.

First-Principles Calculations

In the first-principles formalism the thermal conductivity of GaAs/AlAs SLs is computed by solving the Boltzmann transport equation in the single mode relaxation time (SMRT) approximation using Eq. 1 below. The thermal conductivity was computed by summing over the heat conducted by all the phonon modes (λ) in the Brillouin zone:

$$k_\alpha = \frac{\hbar^2}{N\Omega k_B T^2} \sum_\lambda c_{\alpha\lambda}^2 \omega_\lambda^2 \bar{n}_\lambda \left(\bar{n}_\lambda + 1\right) \tau_\lambda \qquad (1)$$

where c, ω, $\bar{n}$, and τ are the phonon group velocities, frequencies, equilibrium populations, and relaxation times, λ represents the vibrational mode labeled by (qj) (q is the wave vector and j the phonon branch), and T, Ω, and N are the temperature, cell volume and size of the q-point mesh used. The scattering rate, $1/\tau_\lambda$, of a phonon mode λ is taken to be the sum of a term describing scattering due to interfacial disorder ($1/\tau_{\lambda a}$) and a term describing anharmonic scattering ($1/\tau_{\lambda b}$) as in Matthiessen's rule.

All ingredients necessary to compute the thermal conductivity, namely the phonon frequencies, group velocities, populations and lifetimes, are derived from first-principles using density functional perturbation theory (DFPT). The second order and third order interatomic force constants needed to estimate the above parameters are taken to be an average of those in pure GaAs and AlAs and these constants are also obtained from DFPT.

The anharmonic scattering rates ($1/\tau_{\lambda b}$) are computed using the lowest-order three-phonon scattering processes in the SMRT approximation via (*47*)

$$\frac{1}{\tau_{\lambda b}} = \pi \sum_{\lambda'\lambda''} |V_3(-\lambda,\lambda',\lambda'')|^2 \times [2(\bar{n}_{\lambda'} - \bar{n}_{\lambda''})\delta\left(\omega(\lambda) + \omega(\lambda') - \omega(\lambda'')\right) + (1+\bar{n}_{\lambda'} + \bar{n}_{\lambda''})\delta\left(\omega(\lambda) - \omega(\lambda') - \omega(\lambda'')\right)] \qquad (2)$$

where $V_3(-\lambda,\lambda',\lambda'')$ is the three-phonon coupling matrix elements or the weighted Fourier transforms of the cubic force constants.

Interface roughness is simulated as a random mixing of Ga and Al atoms in a narrow region around the interface; this mass-mixing is the dominant interfacial scattering mechanism for phonons at short periods (*21,48*). To compute the interfacial scattering rates, we replace the disordered crystal with an ordered one and treat the disorder as a perturbation (*49*) (an idea first proposed by Abeles (*50*) for alloys); the use of perturbation theory to compute scattering rates due to mass disorder has been found to yield excellent agreement with experiments (*51*). In this perturbative approach, for any SL unit cell the masses of the atoms at sites affected by the disorder are taken to be an average of Ga and Al masses, and the other atoms on either side of the interface are assigned their true masses. We take the thickness of the disordered region to be two layers total consisting of one layer of AlAs and one layer of GaAs with random mixing of Ga and Al atoms. This assumption is consistent with HRTEM images, such as Fig. 1A, and with previous microscopy studies of GaAs/AlAs interfaces (*21*). The phonon modes of this unit cell are used to compute the frequencies, group velocities, populations and lifetimes that enter into the calculation of the thermal conductivity. The scattering rates due to interfacial disorder are calculated using:

$$\frac{1}{\tau_{\lambda a}} = \frac{\pi}{2N}\omega_\lambda^2 \sum_{\lambda'} \delta(\omega_\lambda - \omega_{\lambda'}) \sum_\sigma g(\sigma) |\vec{e}(\sigma|\lambda')\vec{e}(\sigma|\lambda)|^2 \qquad (3)$$

where σ denotes the atomic sites in the SL unit cell, g takes into account the magnitude of the mass disorder and is defined as $g(\sigma) = \sum_i f_i(\sigma)[1 - m_i(\sigma)/\overline{m_i}(\sigma)]^2$ where i, f and m denote the atomic species, concentration and mass, respectively. $\overline{m}(\sigma)$ is the average mass at site σ and e represents the vibration eigenvector. $g(\sigma)$ is non-zero only for atomic sites in the region of disorder; the above equation therefore allows us to compute the phonon scattering due to sub-lattice disorder which is the case for interfacial disorder.

The harmonic force constants are obtained on a 10x10x10 supercell, respectively. The anharmonic force constants are obtained by using a supercell approach as outlined by Esfarjani et al (*52*). For all DFPT calculations, a 8x8x8 Monkhorst-Pack (*53*) mesh is used to sample electronic states in the Brillouin zone and an energy cutoff of 72 Ry is used for the plane-wave expansion. We carefully tested the convergence of all measured quantities with respect to these parameters. First-principles calculations within density-functional theory are carried out using the PWscf and PHonon codes of the Quantum-ESPRESSO distribution (*54*) with norm-conserving pseudopotentials based on the approach of von Barth and Car (*55*).

The above formalism was first used to compute the thermal conductivity of SLs with periods 1.1, 1.6 and 2.2 nm. Calculation of phonon scattering rates beyond a period of 2.2 nm was found to be prohibitively expensive. To compute the thermal conductivity of the 24 nm period SL, we took the anharmonic rates to be the same as in the 2.2 nm SL, since they were found to remain unchanged as the period was increased from 1.6 to 2.2 nm. The interfacial scattering rates, however, were found to scale inversely with the period; for the 24 nm period SL these were therefore obtained by scaling the rates computed for the 2.2 nm period SL.

Figure S3 shows the phonon dispersion along the thickness direction of the 12 nm x 12nm GaAs/AlAs SL. Only lower frequency phonons are shown. In this region, according to Fig. 3, interface scattering is weaker than phonon-phonon scattering and phonon transport across the measured SLs is ballistic. The coherent effects are reflected in the minigaps and modified group velocity of the phonons in the SLs.

Transmission and Green's Function Calculations

The thermal conductance of the super lattice structure is calculated using the Landauer formula (*19*) based on the transmission function. The latter is calculated using the Green's function (GF) formalism detailed in (*38,39*). Fast algorithms are used (*56,57*) to compute the effects of the GaAs substrate and the Al capping layer which are both considered as semi-infinite leads. Since the considered model is harmonic, three-phonon processes are excluded and thus it is assumed that the total thermal resistance comes from phonon scatterings at interfaces due either to roughness or acoustic impedance mismatch. When this formalism is applied to phonons, the energy argument E needs to be

substituted by the square of the phonon frequency ω^2, and the Hamiltonian matrix by the force constant matrix. Due to the translational invariance of the system along the transverse direction, the harmonic problem can be decoupled into N independent chains, one for each considered transverse k vector. The resulting formula for the thermal conductance becomes:

$$G_{ballistic} = \sum_{m,k_t} \frac{1}{N} \int_0^\infty \frac{d\omega}{2\pi} C_v(\omega/T) \Xi_m(k_t,\omega) = \kappa \frac{A}{L} \qquad (4)$$

where C_v is the heat capacity per mode ($C_v = \hbar\omega \frac{\partial n}{\partial T} = \left(\frac{x}{shx}\right)^2$ with $x = \frac{\hbar\omega}{2k_B T}$), and Ξ is the transmission function of a phonon of frequency ω and transverse momentum k_t.

In the plot of Fig. 3(A) in the main paper, the transmission function is divided by the cross section area of the considered 3x3 supercell, and summed over all transverse modes, in order to get the total transmission at a given frequency, per unit area. In the limit of elastic scattering, the transmission function is given by:

$$\Xi(k_t,\omega) = Tr\left[G\Gamma_L G^\dagger \Gamma_R\right] \qquad (5)$$

In this formula, G is the GF of the whole system projected on the SL volume, and the Γs are the escape rates to the left (GaAs) or right (Al) leads. To convert conductance to conductivity, we multiply the former by the system length and divide by its cross section area. To model rough interfaces, we consider one unit cell on the left and one unit cell on the right of the interface, and randomly shuffle their Al and Ga atoms, while maintaining the As atoms at their original positions. This shuffling therefore covers a thickness of about 1 nm, given that the unit cell length on each side is about 0.54 nm.

In the case of clean interfaces, we only need to consider one unit cell in the transverse direction and we perform the summation over k_t defined on a fine mesh (30x30). The cross sectional area of the unit cell is 0.38 nm x 0.38 nm. For rough interfaces, where Ga and Al atoms are randomly shuffled within a layer of the interface, the adopted transverse cell is 3x3 (9 times larger), and the summation is over a 10x10 k_t mesh. In addition, we perform an averaging of the obtained transmissions over 9 sets of randomly generated atomic configurations. We also performed similar calculations for a 6x6 transverse cell and did not see any difference in the average transmissions, and we therefore kept the supercell size of 3x3 for the rest of the calculations.

For the calculations of the force constants (FC) appearing in the Greens functions, we adopted a simple two-nearest neighbor FC model for all three materials: GaAs, AlAs, and Al. It produced a very reasonable band structure and phonon density of states for these materials with the correct bandwidth. The speeds of sound were however off by 10-20% depending on the considered material and direction. The obtained DOS and transmission function can be seen in the following figure (Fig. S4).

The reason for using semiempirical force constants as opposed to first-principles ones was simply their ease of use. In case we need to artificially modify the force constants or make the correct connection of the Al lattice to GaAs which has a different coordination

number, the use of an analytical formula is much more convenient. Even though our goal here was not to get exact quantitative agreement with the experiment but was instead to show qualitatively the trends, the used force constants yield very reasonable band structure and transmission values. The transmission calculations were done for a size similar to the real experiment: SLs of 1,3,5,7,9 periods were made, in which each period consisted of 22 unit cells of GaAs and 22 unit cells of AlAs, resulting in a period of 23.76 nm containing 176 atoms per unit cell.

Author Contributions:

M. N. Luckyanova performed the TDTR experiments. J. Garg conducted the first-principles calculations. K. Esfarjani conducted Green's functions calculations. A. Jandl, M. T. Bulsara and E. A. Fitzgerald grew the samples used in the experiments. A. J. Minnich and M. S. Dresselhaus, participated in discussions. A. J. Schmidt assisted with the experiments. S. Chen and Z.F. Ren provided the HRTEM image. G. Chen supervised the research and contributed to data interpretation. M. N. Luckyanova, J. Garg, K. Esfarjani, and G. Chen wrote the paper.

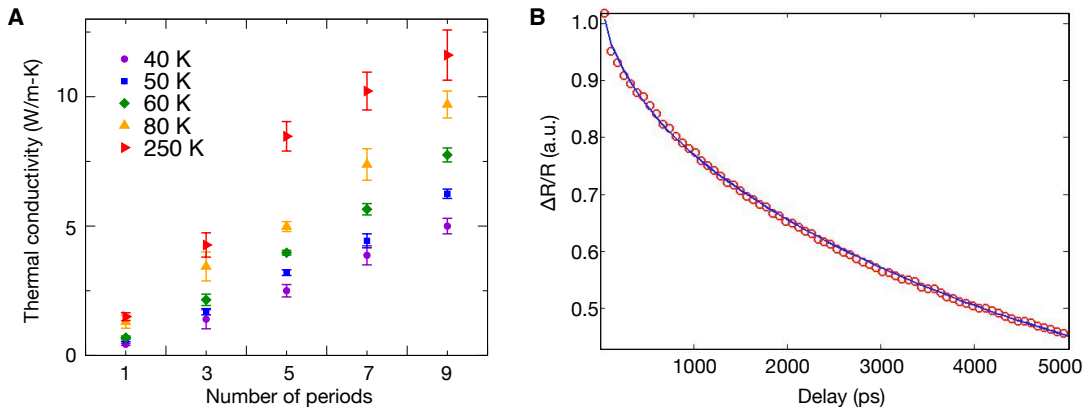

Fig. S1.

(A) Thermal conductivities of SLs at five temperatures. The error bars represent the standard deviations of 20 average thermal conductivity values for each point. (B) A sample data set (open circles) and fitting curve (solid line) for a five period SL at 150K and 3 MHz modulation.

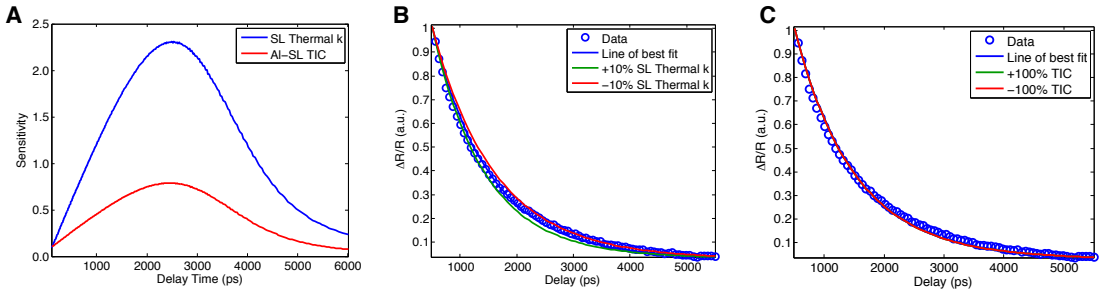

Fig. S2

(A) Sensitivity analysis for a 1-pd SL sample at 30K. This analysis shows that for all times, the fitting is more sensitive to the thermal conductivity of the SL rather than the thermal interface conductance. (C) Data for a 1-pd SL sample at 30K and 6 MHz pump modulation frequency. The blue open circles are data points, the blue line represents the line of best fit, the green and red solid lines are the best fit lines if the SL thermal conductivity is varied by +/-10%. (C) Data for the same sample as in (B) where, again, the blue line represents the line of best fit and the red and green lines represent the lines of best fit if the Al-SL thermal interface conductance is varied by +/-100%.

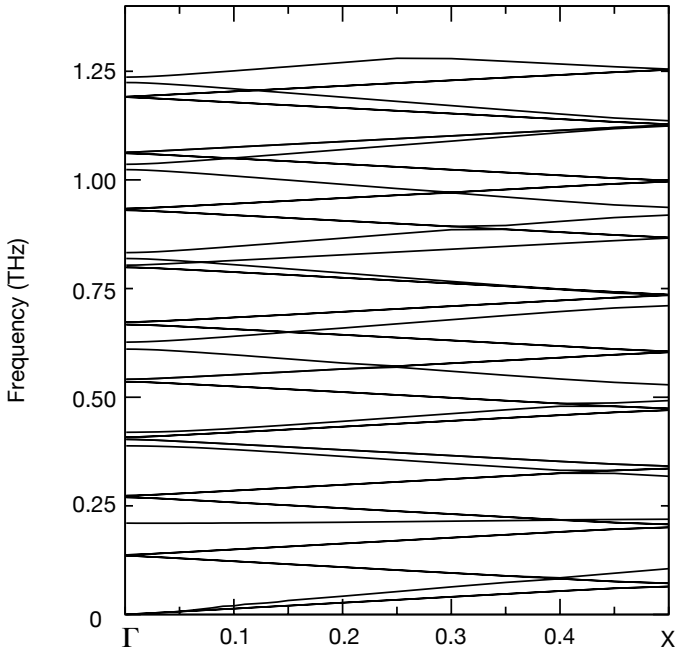

Fig. S3

Phonon dispersion of the 24 nm period GaAs/AlAs superlattice along Γ-X. Only low frequency phonon modes are shown. This dispersion which incorporates the coherence effects as indicated by the phonon band gaps is used for computing the thermal conductivity.

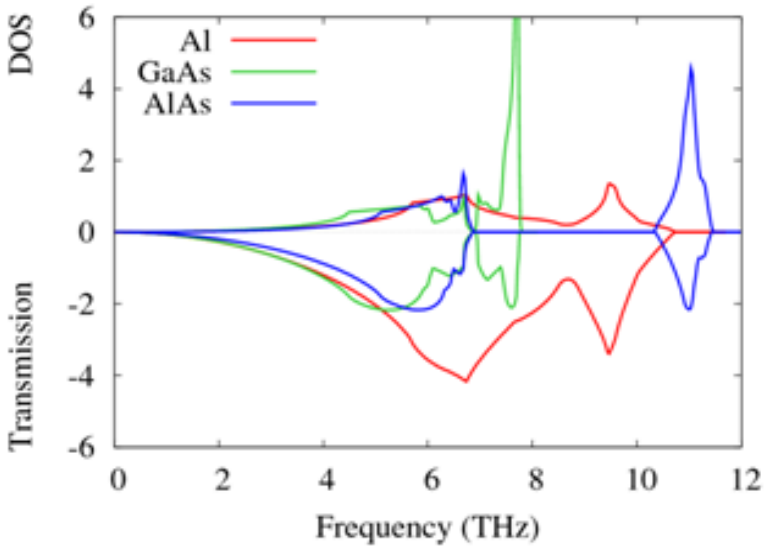

Fig. S4

Phonon density of states (top) and negative of the transmission function (bottom) for the three considered bulk structures. For an ideal infinite system, the transmission is essentially the DOS multiplied by the group velocity in the transport direction (100). For clarity, the transmission function has been plotted below the x axis. It is the total transmission within a 0.38 nm x 0.38 nm unit cell, summed over all transverse momenta.

References

1. D. G. Cahill *et al*., Nanoscale thermal transport. *J. Appl. Phys.* **93**, 793 (2003). doi:10.1063/1.1524305

2. H. B. G. Casimir, Note on the conduction of heat in crystals. *Physica* **5**, 495 (1938). doi:10.1016/S0031-8914(38)80162-2

3. J.-K. Yu, S. Mitrovic, D. Tham, J. Varghese, J. R. Heath, Reduction of thermal conductivity in phononic nanomesh structures. *Nat. Nanotechnol.* **5**, 718 (2010). doi:10.1038/nnano.2010.149 Medline

4. C. W. Chang, D. Okawa, A. Majumdar, A. Zettl, Solid-state thermal rectifier. *Science* **314**, 1121 (2006). doi:10.1126/science.1132898 Medline

5. J. Lim, K. Hippalgaonkar, S. C. Andrews, A. Majumdar, P. Yang, Quantifying surface roughness effects on phonon transport in silicon nanowires. *Nano Lett.* **12**, 2475 (2012). doi:10.1021/nl3005868 Medline

6. C. Colvard, R. Merlin, M. V. Klein, A. C. Gossard, Observation of folded acoustic phonons in a semiconductor superlattice. *Phys. Rev. Lett.* **45**, 298 (1980). doi:10.1103/PhysRevLett.45.298

7. J. Wang *et al*., Propagating coherent acoustic phonon wave packets in $In_xMn_{1-x}As$/GaSb. *Phys. Rev. B* **72**, 153311 (2005). doi:10.1103/PhysRevB.72.153311

8. V. Narayanamurti, H. L. Störmer, M. A. Chin, A. C. Gossard, W. Wiegmann, Selective transmission of high-frequency phonons by a superlattice: The “dielectric” phonon filter. *Phys. Rev. Lett.* **43**, 2012 (1979). doi:10.1103/PhysRevLett.43.2012

9. V. Narayanamurti, Phonon optics and phonon propagation in semiconductors. *Science* **213**, 717 (1981). doi:10.1126/science.213.4509.717 Medline

10. S. Tamura, D. C. Hurley, J. P. Wolfe, Acoustic-phonon propagation in superlattices. *Phys. Rev. B* **38**, 1427 (1988). doi:10.1103/PhysRevB.38.1427

11. T. Yao, Thermal properties of AlAs/GaAs superlattices. *Appl. Phys. Lett.* **51**, 1798 (1987). doi:10.1063/1.98526

12. X. Y. Yu, G. Chen, A. Verma, J. S. Smith, Temperature dependence of thermophysical properties of GaAs/AlAs periodic structure. *Appl. Phys. Lett.* **67**, 3554 (1995). doi:10.1063/1.114919

13. W. S. Capinski *et al*., Thermal-conductivity measurements of GaAs/AlAs superlattices using a picosecond optical pump-and-probe technique. *Phys. Rev. B* **59**, 8105 (1999). doi:10.1103/PhysRevB.59.8105

14. S.-M. Lee, D. G. Cahill, R. Venkatasubramanian, Thermal conductivity of Si–Ge superlattices. *Appl. Phys. Lett.* **70**, 2957 (1997). doi:10.1063/1.118755

15. G. Chen, Thermal conductivity and ballistic-phonon transport in the cross-plane direction of superlattices. *Phys. Rev. B* **57**, 14958 (1998). doi:10.1103/PhysRevB.57.14958

16. B. C. Daly, H. J. Maris, K. Imamura, S. Tamura, Molecular dynamics calculation of the thermal conductivity of superlattices. *Phys. Rev. B* **66**, 024301 (2002). doi:10.1103/PhysRevB.66.024301

17. Y. K. Koh, Y. Cao, D. G. Cahill, D. Jena, Heat-transport mechanisms in superlattices. *Adv. Funct. Mater.* **19**, 610 (2009). doi:10.1002/adfm.200800984

18. E. T. Swartz, R. O. Pohl, Thermal boundary resistance. *Rev. Mod. Phys.* **61**, 605 (1989). doi:10.1103/RevModPhys.61.605

19. R. Landauer, Electrical resistance of disordered one-dimensional lattices. *Philos. Mag.* **21**, 863 (1970). doi:10.1080/14786437008238472

20. D. Li *et al*., Thermal conductivity of individual silicon nanowires. *Appl. Phys. Lett.* **83**, 2934 (2003). doi:10.1063/1.1616981

21. P. D. Robb, A. J. Craven, Column ratio mapping: a processing technique for atomic resolution high-angle annular dark-field (HAADF) images. *Ultramicroscopy* **109**, 61 (2008). doi:10.1016/j.ultramic.2008.08.001 Medline

22. C. A. Paddock, G. L. Eesley, Transient thermoreflectance from thin metal films. *J. Appl. Phys.* **60**, 285 (1986). doi:10.1063/1.337642

23. D. G. Cahill, Analysis of heat flow in layered structures for time-domain thermoreflectance. *Rev. Sci. Instrum.* **75**, 5119 (2004). doi:10.1063/1.1819431

24. A. J. Schmidt, X. Chen, G. Chen, Pulse accumulation, radial heat conduction, and anisotropic thermal conductivity in pump-probe transient thermoreflectance. *Rev. Sci. Instrum.* **79**, 114902 (2008). doi:10.1063/1.3006335 Medline

25. Materials and methods are available as supplementary materials on *Science* Online.

26. M. A. Afromowitz, Thermal conductivity of Ga1−xAlxAs alloys. *J. Appl. Phys.* **44**, 1292 (1973). doi:10.1063/1.1662342

27. P. Hyldgaard, G. D. Mahan, Phonon superlattice transport. *Phys. Rev. B* **56**, 10754 (1997). doi:10.1103/PhysRevB.56.10754

28. S. Tamura, Y. Tanaka, H. J. Maris, Phonon group velocity and thermal conduction in superlattices. *Phys. Rev. B* **60**, 2627 (1999). doi:10.1103/PhysRevB.60.2627

29. E. S. Landry, A. J. H. McGaughey, Effect of interfacial species mixing on phonon transport in semiconductor superlattices. *Phys. Rev. B* **79**, 075316 (2009). doi:10.1103/PhysRevB.79.075316

30. S. Volz, J. B. Saulnier, G. Chen, P. Beauchamp, Computation of thermal conductivity of Si/Ge superlattices by molecular dynamics techniques. *Microelectron. J.* **31**, 815 (2000). doi:10.1016/S0026-2692(00)00064-1

31. S. Baroni, P. Giannozzi, A. Testa, Green's-function approach to linear response in solids. *Phys. Rev. Lett.* **58**, 1861 (1987). doi:10.1103/PhysRevLett.58.1861 Medline

32. D. A. Broido, M. Malorny, G. Birner, N. Mingo, D. A. Stewart, Intrinsic lattice thermal conductivity of semiconductors from first principles. *Appl. Phys. Lett.* **91**, 231922 (2007). doi:10.1063/1.2822891

33. K. Esfarjani, G. Chen, H. T. Stokes, Heat transport in silicon from first-principles calculations. *Phys. Rev. B* **84**, 085204 (2011). doi:10.1103/PhysRevB.84.085204

34. J. Garg, N. Bonini, B. Kozinsky, N. Marzari, Role of disorder and anharmonicity in the thermal conductivity of silicon-germanium alloys: A first-principles study. *Phys. Rev. Lett.* **106**, 045901 (2011). doi:10.1103/PhysRevLett.106.045901 Medline

35. J. Garg, N. Bonini, N. Marzari, High thermal conductivity in short-period superlattices. *Nano Lett.* **11**, 5135 (2011). doi:10.1021/nl202186y Medline

36. S. Tamura, Isotope scattering of dispersive phonons in Ge. *Phys. Rev. B* **27**, 858 (1983). doi:10.1103/PhysRevB.27.858

37. P. A. Lee, D. S. Fisher, Anderson localization in two dimensions. *Phys. Rev. Lett.* **47**, 882 (1981). doi:10.1103/PhysRevLett.47.882

38. C. Caroli, R. Combescot, P. Nozieres, D. Saint-James, Direct calculation of the tunneling current. *J. Phys. C Solid State Phys.* **4**, 916 (1971). doi:10.1088/0022-3719/4/8/018

39. Y. Meir, N. S. Wingreen, Landauer formula for the current through an interacting electron region. *Phys. Rev. Lett.* **68**, 2512 (1992). doi:10.1103/PhysRevLett.68.2512 Medline

40. G. Pernot *et al*., Precise control of thermal conductivity at the nanoscale through individual phonon-scattering barriers. *Nat. Mater.* **9**, 491 (2010). doi:10.1038/nmat2752 Medline

41. R. M. Costescu, D. G. Cahill, F. H. Fabreguette, Z. A. Sechrist, S. M. George, Ultra-low thermal conductivity in W/Al2O3 nanolaminates. *Science* **303**, 989 (2004). doi:10.1126/science.1093711 Medline

42. C. Chiritescu *et al*., Ultralow thermal conductivity in disordered, layered WSe2 crystals. *Science* **315**, 351 (2007). doi:10.1126/science.1136494 Medline

43. A. Schmidt, M. Chiesa, X. Chen, G. Chen, An optical pump-probe technique for measuring the thermal conductivity of liquids. *Rev. Sci. Instrum.* **79**, 064902 (2008). doi:10.1063/1.2937458 Medline

44. A. J. Schmidt, X. Chen, G. Chen, Pulse accumulation, radial heat conduction, and anisotropic thermal conductivity in pump-probe transient thermoreflectance. *Rev. Sci. Instrum.* **79**, 114902 (2008). doi:10.1063/1.3006335 Medline

45. B. C. Gundrum, D. G. Cahill, R. S. Averback, Thermal conductance of metal-metal interfaces. *Phys. Rev. B* **72**, 245426 (2005). doi:10.1103/PhysRevB.72.245426

46. A. J. Minnich, G. Chen, S. Mansoor, B. S. Yilbas, Quasiballistic heat transfer studied using the frequency-dependent Boltzmann transport equation. *Phys. Rev. B* **84**, 235207 (2011). doi:10.1103/PhysRevB.84.235207

47. G. Deinzer, G. Birner, D. Strauch, Ab initio calculation of the linewidth of various phonon modes in germanium and silicon. *Phys. Rev. B* **67**, 144304 (2003). doi:10.1103/PhysRevB.67.144304

48. S. P. Hepplestone, G. P. Srivastava, Theory of interface scattering of phonons in superlattices. *Phys. Rev. B* **82**, 144303 (2010). doi:10.1103/PhysRevB.82.144303

49. S. Tamura, Isotope scattering of dispersive phonons in Ge. *Phys. Rev. B* **27**, 858 (1983). doi:10.1103/PhysRevB.27.858

50. B. Abeles, Lattice thermal conductivity of disordered semiconductor alloys at high temperatures. *Phys. Rev.* **131**, 1906 (1963). doi:10.1103/PhysRev.131.1906

51. W. A. Kamitakahara, B. N. Brockhouse, Vibrations of a mixed crystal: Neutron scattering from Ni_55Pd_45. *Phys. Rev. B* **10**, 1200 (1974). doi:10.1103/PhysRevB.10.1200

52. K. Esfarjani, H. T. Stokes, Method to extract anharmonic force constants from first principles calculations. *Phys. Rev. B* **77**, 144112 (2008). doi:10.1103/PhysRevB.77.144112

53. H. J. Monkhorst, J. D. Pack, Special points for Brillouin-zone integrations. *Phys. Rev. B* **13**, 5188 (1976). doi:10.1103/PhysRevB.13.5188

54. P. Giannozzi *et al*., QUANTUM ESPRESSO: A modular and open-source software project for quantum simulations of materials. *J. Phys. Condens. Matter* **21**, 395502 http://www.quantum-espresso.org (2009). doi:10.1088/0953-8984/21/39/395502 Medline

55. A. Dal Corso, S. Baroni, R. Resta, S. de Gironcoli, Ab initio calculation of phonon dispersions in II-VI semiconductors. *Phys. Rev. B* **47**, 3588 (1993). doi:10.1103/PhysRevB.47.3588

56. M. P. Lopez-Sancho, J. M. Lopez-Sancho, J. Rubio, Quick iterative scheme for the calculation of transfer matrices: application to Mo (100). *J. Phys. F Met. Phys.* **14**, 1205 (1984). doi:10.1088/0305-4608/14/5/016

57. M. P. Lopez-Sancho, J. M. Lopez-Sancho, J. Rubio, Highly convergent schemes for the calculation of bulk and surface Green functions. *J. Phys. F Met. Phys.* **15**, 851 (1985). doi:10.1088/0305-4608/15/4/009